Available online at www.sciencedirect.com
SCIENCE DIRECT®
International Journal of Heat and Fluid Flow 24 (2003) 500–511
International Journal of HEAT AND FLUID FLOW
www.elsevier.com/locate/ijhff

A numerical study on the eddy structures of impinging jets excited at the inlet

M. Tsubokura [a,*], T. Kobayashi [b], N. Taniguchi [b], W.P. Jones [c]

[a] Department of Environmental Science and Technology, Tokyo Institute of Technology, 4259 Nagatsuta, Midoriku, Yokohamashi 226-8502, Japan
[b] Institute of Industrial Science, University of Tokyo, 4-6-1 Komaba, Meguroku 153-8505, Japan
[c] Department of Mechanical Engineering, Imperial College London, London SW7 2AX, UK

Received 3 December 2002; accepted 12 March 2003

Abstract

Three-dimensional eddy structures arising in plane and round impinging jets excited at the nozzle inlet were investigated numerically by direct numerical simulation and large eddy simulation. Special attention is focused on how spanwise or azimuthal disturbances imposed at the inlet velocity affect the eddy structures in the transition process. In this respect, three spatial wavelength of $\lambda/\pi D = 1/3$, 1/4 and 1/6, where D is the nozzle width or the diameter, were tested in this study. It was found that the round jet showed definite instability at $\lambda/\pi D = 1/6$ while the plane jet showed almost equivalent sensitivity to all modes tested here. As regards the eddy structures in the stagnation region, elongated twin vortices along the impinging plate of the plane jet were reproduced and the number of pairs was found to agree exactly with the spanwise wave number imposed at the inlet. In contrast to the plane jet, no organized structures were observed in the stagnation region of the round jet.

Keywords: Impinging jet; Eddy structures; Direct numerical simulation; Large eddy simulation; Stagnation; Instability; Transition

1. Introduction

Impinging jet flow is of great interest in industrial applications because it is often utilized to heat, cool or dry materials. The reason of such utilization in the processing of materials is that the flow results in high heat and mass conductivity in the stagnation region. This feature has led many researchers to study impinging jets from the standpoint of heat and mass transfer (rather than the fluid dynamics), and to propose empirical equations which relate heat or mass transfer rates, Reynolds number, distance between the nozzle and the impinging plate and so on (e.g., Martin, 1977).

In addition, stagnation flow is also interesting as a physical phenomenon because strong shrinking and stretching in this region produces a characteristic eddy structure. In case of the plane impinging jet (which is sometimes called Hiemenz flow), Sutera et al. (1963, 1965) proposed that the high heat transfer is caused by the stretched vortex aligned parallel to the wall. Yokobori et al. (1983) studied the plane impinging jet experimentally using a flow visualization technique and observed counter-rotating vortex pairs along the wall. They also measured the temperature distribution and found that the high heat transfer rate is related to these counter-rotating twin vortices. Sakakibara et al. (1997, 2001) further studied the plane impinging jet using simultaneous measurements of velocity and temperature fields by digital particle image velocimetry (PIV) and laser-induced fluorescence (LIF) and found that the counter-rotating vortex pairs are convected from an upstream location and stretched in the vicinity of the wall. However the relation or sensitivity of the inlet condition and these vortex structures at the stagnation is not yet fully understood. In contrast to the plane jet, few studies on the eddy structures in the stagnation region of the round impinging jet have been conducted until recently (e.g., Satake and Kunugi, 1998).

* Corresponding author. Present address: Department of Mechanical Engineering and Intelligent Systems, The University of Electro-Communications, Chofugaoka 1-5-1, Chofu-shi, Tokyo 182-8585, Japan.
E-mail address: tsubo@mce.uec.ac.jp (M. Tsubokura).

0142-727X/03/$ - see front matter © 2003 Elsevier Science Inc. All rights reserved.
doi:10.1016/S0142-727X(03)00044-4

Direct numerical simulation (DNS) and large eddy simulation (LES) are useful methods to investigate such eddy structures. DNS essentially simulates the complete turbulence structure instantaneously while in LES the large-scale structures are computed directly with only the small scales being modelled. In previous studies (Tsubokura et al., 1996, 1997), an LES method has been developed which is suitable for simulating such a complicated flow (consisting of both free and wall turbulent shear regions, transition from laminar to turbulent flow and an impinging region) and applied it to study the three dimensional organized structures of a plane impinging jet at a Reynolds number of 6000 (Tsubokura et al., 1998). In the present study, attention is focused on the differences in the eddy structures of plane and round jets excited at the inlet. The Reynolds numbers (Re), based on the nozzle width or diameter and the inlet velocity at the nozzle, adopted here are 2000 for the DNS and 6000 for the LES.

2. Numerical method

2.1. Plane and round impinging jets

Plane and round jets impinging normally onto a flat plate are shown in Fig. 1. The flat plate is mounted at a distance of $10D$ away from the nozzle exit in both cases, where D is the width or the diameter of the nozzles. A Cartesian coordinate system with origin in the middle of the stagnation line on the plate is used for the plane jet, where x, y and z represent the transverse, normal-wall and spanwise directions respectively. For the round jet, a cylindrical polar coordinate system with origin at the stagnation point is used where y is the axial (normal-wall), r is the radial and θ is the azimuthal direction. The analysis regions for the plane jet corresponds to $0 \leqslant x \leqslant 53D$, $0 \leqslant y \leqslant 10D$ and $0 \leqslant z \leqslant \pi D$ while those for round jets are $0 \leqslant y \leqslant 10D$, $0 \leqslant r \leqslant 18D$ and $0 \leqslant \theta \leqslant 2\pi$. The total grid number used for both DNS (lower Re case) and LES (higher Re case) in this study is $N_x \times N_y \times N_z = 400 \times 100 \times 96$ in plane and $N_y \times N_r \times N_\theta = 100 \times 150 \times 96$ in round jets.

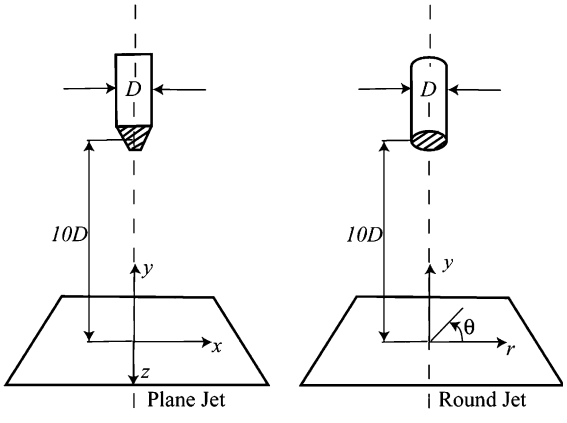

Fig. 1. Analysis models.

The numerical grids are stretched at the shear-layer with a finer grid width being considered in LES for the higher Re case.

2.2. Governing equations

The incompressible Navier–Stokes and continuity equations are the governing equations for DNS in this study, while these equations are spatially filtered to obtain the governing equations for LES. The filtered continuity and Navier–Stokes equations are:

$$\nabla \cdot \bar{\boldsymbol{u}} = 0, \tag{1}$$

$$\frac{\partial \bar{\boldsymbol{u}}}{\partial t} + \nabla \cdot (\bar{\boldsymbol{u}} \otimes \bar{\boldsymbol{u}}) = -\nabla \overline{P} + \nabla \cdot \left\{ (\nu + \nu_{\mathrm{sgs}})(\nabla \bar{\boldsymbol{u}}) \right\} + \nabla \cdot \left\{ (\nu + \nu_{\mathrm{sgs}})(\nabla \bar{\boldsymbol{u}})^{\mathrm{T}} \right\}, \tag{2}$$

in which ν_{sgs} is the subgrid-scale (SGS) eddy viscosity coefficient to be modelled. An isotropic eddy viscosity model is adopted here, in which ν_{sgs} is modelled as follows:

$$\nu_{\mathrm{sgs}} = C\overline{\Delta}\frac{|\bar{\boldsymbol{u}} - \bar{\bar{\boldsymbol{u}}}|}{3}. \tag{3}$$

The validity of this isotropic model compared with the standard Smagorinsky model has been demonstrated in a simple fully developed plane channel flow by Yoshizawa et al. (1996) and Tsubokura (2001).

In addition to the equations above, the transport equation for a passive scalar is also solved in order to investigate dispersion and mixing mechanisms, as well as to visualize the flow-field. This is:

$$\frac{\partial \overline{\phi}}{\partial t} + \nabla \cdot (\bar{\boldsymbol{u}}\overline{\phi}) = \nabla \cdot \left\{ (\alpha + \alpha_{\mathrm{sgs}})(\nabla \overline{\phi}) \right\}. \tag{4}$$

In Eq. (4) α_{sgs} is the SGS eddy diffusivity coefficient. The eddy diffusivity is modelled in an analogous manner to the eddy viscosity and the SGS Schmidt number is an important parameter to determine the SGS turbulent mixing of the passive scalar:

$$\alpha_{\mathrm{sgs}} = \frac{\nu_{\mathrm{sgs}}}{Sc_{\mathrm{sgs}}}. \tag{5}$$

In the present study, both the model coefficient C appearing in Eq. (3) and the SGS Schmidt number Sc_{sgs} are determined by the dynamic procedure proposed by Germano et al. (1991) and Lilly (1992). The Lagrangian averaging technique proposed by Meneveau et al. (1996) has been adopted to avoid instability induced by the possible negative eddy viscosities or diffusivities arising from the dynamic procedure.

2.3. Discretization

The governing Eqs. (1), (2) and (4) are discretized using a finite difference technique. All space derivatives are discretized using second order central differences, i.e. no artificial viscosity or an upwind type scheme is considered for the convective term, while fully explicit time marching is conducted using a third order Runge–Kutta scheme. The MAC method is adopted to handle the coupling between the velocity and pressure. The resulting Poisson equation for pressure is solved by FFT for the statistically homogeneous direction, i.e. the spanwise or azimuthal direction, while the incomplete Cholesky decomposed conjugant gradient method, ICCG, is adopted for the other two inhomogeneous directions.

2.4. Inlet forcing and other boundary conditions

Transition or the evolution of jets is strongly affected by the inlet condition at the nozzle exit. In the present study, nozzle flows are not explicitly solved, but treated by prescribing an assumed velocity profile at the nozzle exit as the inlet boundary condition. A disturbance is artificially added to the assumed mean velocity profile at the nozzle exit plane. Both jets are forced unsteadily by adding a streamwise sinusoidal disturbance uniformly in the streamwise direction at the Strouhal number $S_t = 0.4$ normalized by the inlet velocity V_0 and nozzle width (or diameter) D. As will be shown in the next section this Strouhal number is close to the natural unstable mode of the shear-layer of both plane and round impinging jets studied here.

In addition to the streamwise disturbance, a spatial periodic disturbance is added in the spanwise or azimuthal direction. The spatial disturbance corresponds to a single sinusoidal wave with the wavelength of λ added to the assumed mean velocity profiles. The amplitude of both the unsteady and the spatial disturbances are 0.5% of V_0. It should be noted that these disturbances are imposed only on the streamwise velocity. The number of waves in the spanwise or the azimuthal direction is varied to investigate how the disturbance affects the structures in the stagnation region of the impinging jets, and three wave numbers of three, four and six are considered. Because both the spanwise length of the plane jet and the circumference of the round jet are set equal to πD at the nozzle exit here, the imposed wavelengths of both plane and round jets are $\lambda = \pi D/3$, $\pi D/4$, $\pi D/6$ respectively.

For the round jet the resulting inlet profile is:

$$V(r,\theta,t)/V_0 = -\left\{1 - (2r/D)^8\right\} + 0.005\sin(2\pi S_t t) + 0.005\sin\left(\frac{\pi D}{\lambda_\theta}\theta\right). \quad (6)$$

The assumed mean velocity profile, described by the first term on the right of Eq. (6), gives boundary-layer and momentum thicknesses of $\delta = 0.22D$ and $\theta = 0.026D$. For the plane jet, the spanwise disturbance is replaced by $0.005\sin(2\pi z/\lambda_z)$.

A convective boundary condition is adopted at the outflow plane while periodic conditions are used in the spanwise direction of the plane jet. The no-slip condition is applied at the wall. The passive scalar is set to unity at the nozzle outlet while the normal gradient of the scalar is set to zero on the wall.

3. Natural instability

3.1. Natural roll-up frequency

The Strouhal number, S_t, is an important parameter in Eq. (6) that serves to phase-lock the position of the roll-up eddies caused by the Kelvin–Helmholtz instability of the shear-layer. The unstable frequency of the shear-layer is mainly determined by the mean velocity profiles, but other factors such as the distance between the nozzle exit and the impinging plate, the size of the analysis region and the outlet condition may affect the unstable mode. Therefore in this section the natural roll-up frequency of the impinging jets is investigated. The sinusoidal perturbation is omitted by setting $S_t = 0$ and $\lambda = 0$ in the inlet profile, Eq. (6), and instead a 3% random perturbation is added to the mean velocity profile.

The power spectra of the streamwise velocity in the shear layer at various heights from the impinging plate are shown in Fig. 2. The round jet shows a distinct unstable mode of $S_t = 0.37$ in contrast to the plane jet which does not show a clear single unstable mode and several modes are equivalently excited in the downstream region. However near the nozzle at $y/D = 8$, the plane jet shows an unstable mode of $S_t = 0.44$. Therefore, as stated in the previous section, the value $S_t = 0.4$ has been selected as the fundamental frequency for the forcing of the impinging jets investigated in this study, as this is close to the natural unstable mode observed both in the plane and round impinging jets tested here.

3.2. Instability in the spanwise/azimuthal directions

The plane or round jet has a natural instability also in the spanwise or the azimuthal direction, which is more important once roll-up eddies appear in the shear layer. This is because these unstable modes determine the number of the rib vortices caused between the roll-up eddies. The natural unstable modes for the spanwise and azimuthal directions of the plane and round jets are sought here and this is achieved by considering the only the fundamental frequency of $S_t = 0.4$ with $\lambda = 0$. Fig. 3 indicates the instantaneous eddy structures observed in the plane and round impinging jets. It can be seen that

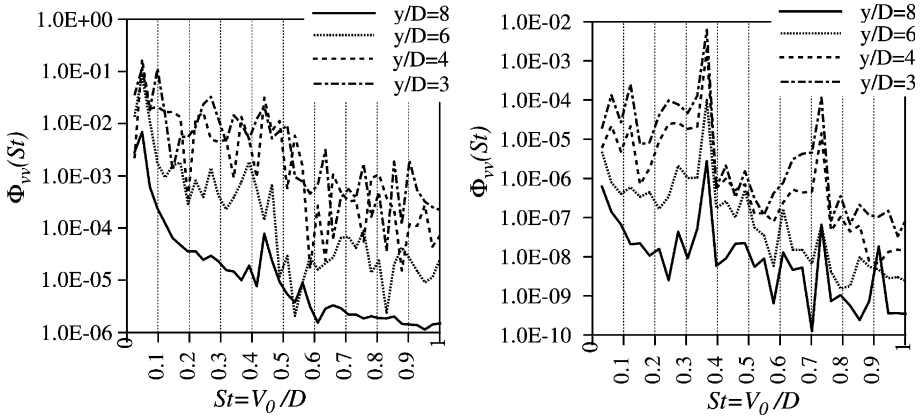

Fig. 2. Power spectra of the streamwise velocity fluctuation at the shear layer: left, plane jet; right, round jet.

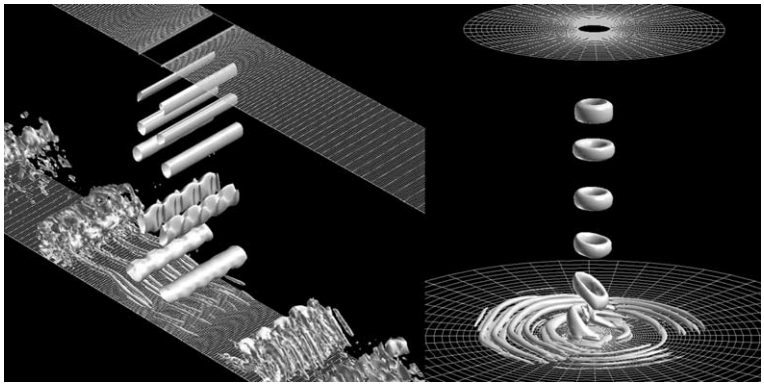

Fig. 3. Instantaneous eddy structures of plane (left) and round (right) impinging jets, indicated by iso-surfaces of the Laplacian of pressure ($\Delta p' = 2.0$), excited by the fundamental frequency of $S_t = 0.4$ ($\lambda = 0$).

spanwise perturbations of four waves are naturally excited downstream and corresponding twin elongated vortices appear near the wall of the plane impinging jet. In contrast the round jet does not show a definite instability in the azimuthal direction and a helical mode seemingly develops near the impinging plate.

As regards the instability in the spanwise or azimuthal directions, the results obtained here agree well with previous theoretical work. The linear stability theory of a periodic row of vortices, as the model of the plane shear layer, conducted by Pierrehumbert and Widnall (1982) showed that the most unstable mode for the spanwise length is approximately 2/3 of the space between roll-up vortex centres. In this study, we have adopted a forcing frequency corresponding to $S_t = 0.4$, in which the space between roll-up vortex centres can be estimated as $\lambda = 1/(2S_t)D = 1.25D$. Accordingly the most unstable spanwise wavelength can be estimated to be about $0.83D$, equivalent to about four waves in our simulation.

In case of the round jet, Batchelor and Gill (1962) predicted from the linear stability theory that at the far downstream of an axisymmetric jet, only the helical mode yielded amplified disturbances.

4. Eddy structures of impinging jets

4.1. Instantaneous structures

Visualized snapshots of the plane and round impinging jets are investigated in this section to determine the overall eddy structures and the fundamental difference between plane and round impinging jets. Fig. 4 shows the instantaneous eddy structures and scalar distribution images on the cross plane (x–z) of a plane jet for different spanwise disturbances. As can be clearly seen the two-dimensional eddies roll up near the inlet, and have a three-dimensional structure due to the spanwise disturbance as the flow evolves downstream. The scalar distribution in each image also shows that the development of spanwise disturbance during the transition is strongly affected by the inlet spanwise forcing and that the wave number of the disturbances is exactly

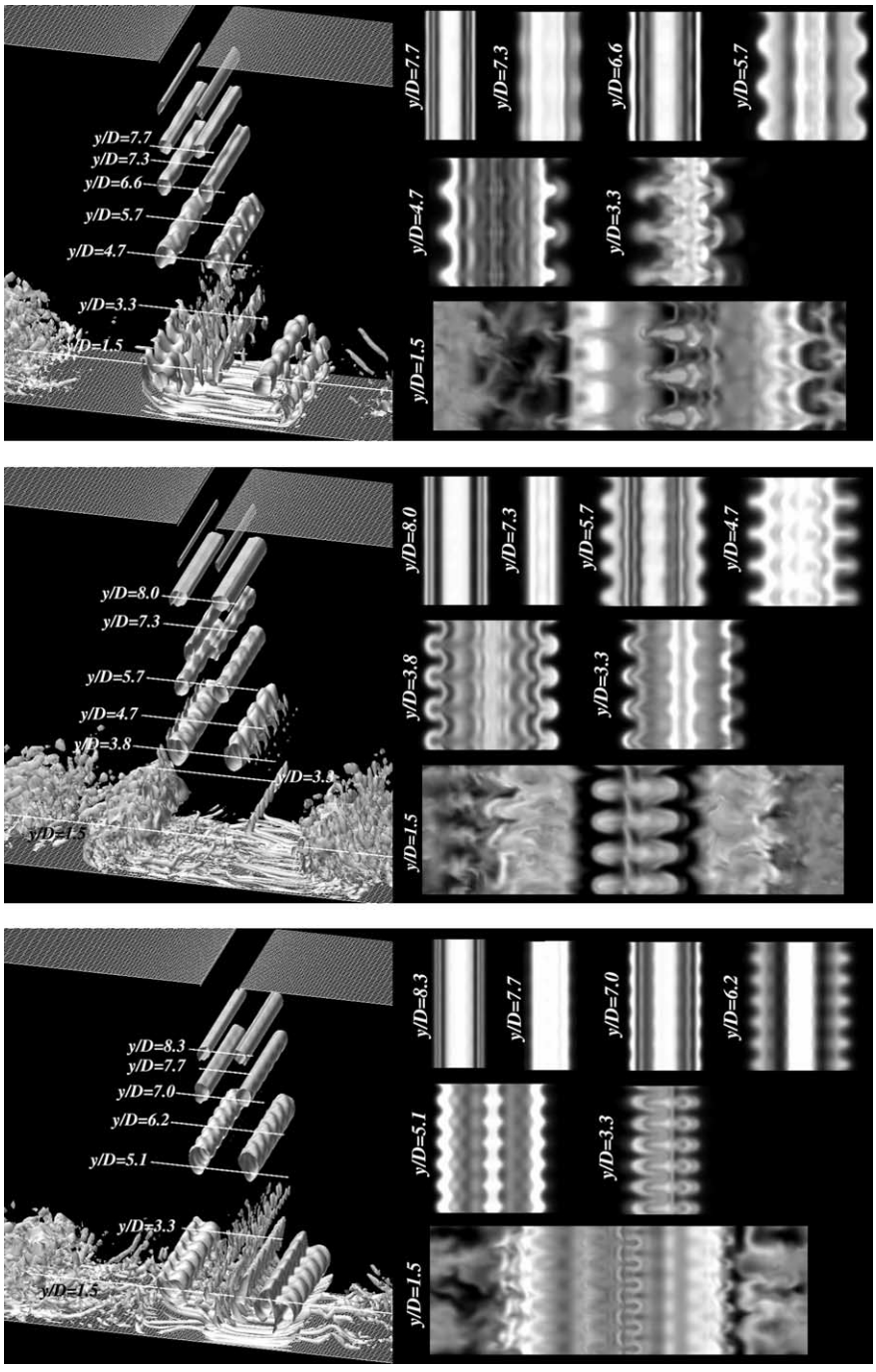

Fig. 4. Instantaneous scalar distribution images (right) and eddy structures indicated by iso-surfaces of the Laplacian of pressure (left, $\Delta p' = 2.0$) in the case of plane jets at various spanwise disturbances: top, $\lambda_z/\pi D = 1/3$; middle, $\lambda_z/\pi D = 1/4$; bottom, $\lambda_z/\pi D = 1/6$; equivalent to three, four and six waves in the spanwise direction respectively. Scalar distributions are illustrated on (x, z) planes at various heights from the impinging wall.

the same as the one imposed in the inlet (three, four and six waves from the top to the bottom respectively in Fig. 4).

On the other hands, the round impinging jet shows a different tendency as regards the development of the azimuthal disturbance (see Fig. 5). In general, the transition process is the same as in the plane jet in the sense that eddies roll up around $y/D = 6$ and the vortex ring develops to show three-dimensional structures as flow goes downstream. However the stability of the imposed azimuthal disturbance is different. When three or six waves are imposed at the inlet of the round jet, the scalar images close to the impinging plate show that six waves are finally developed (the same star-like scalar distributions having six ridges can be seen at the plane $y/D = 1.6$ on the top and at $y/D = 2.1$ at the bottom of

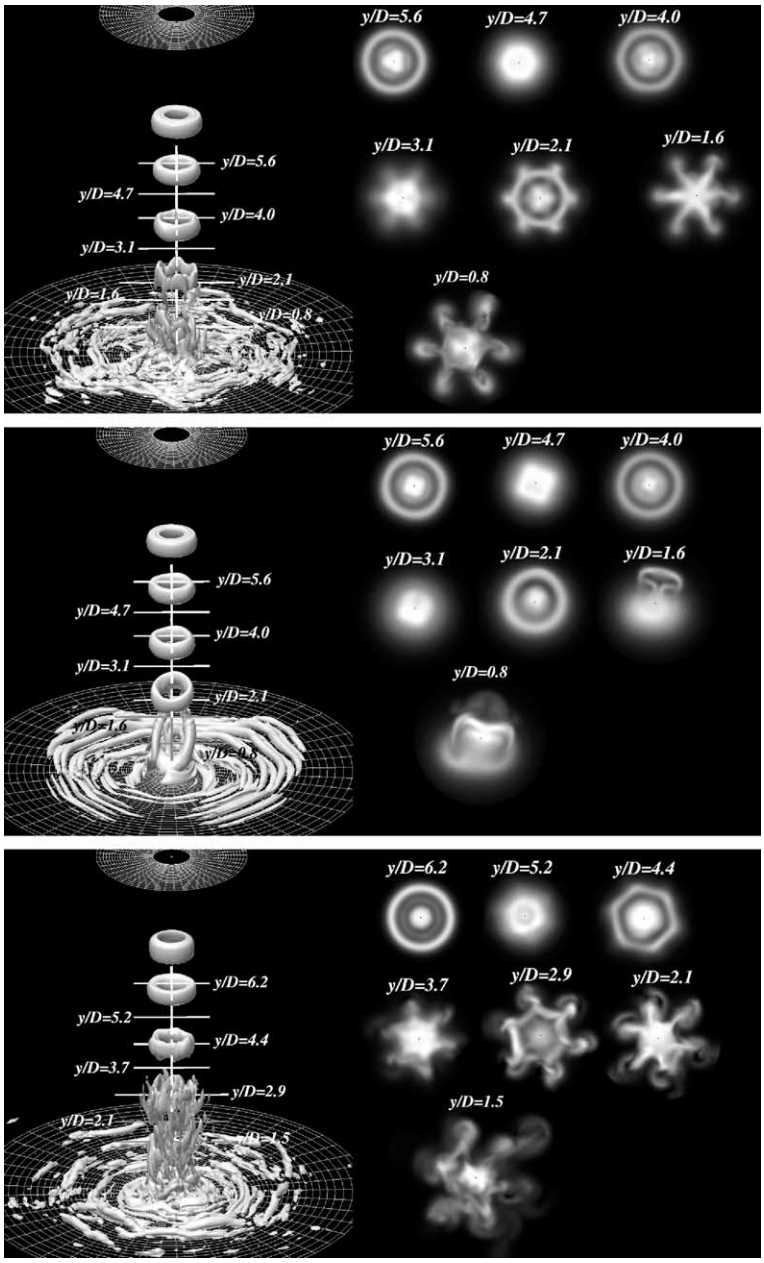

Fig. 5. Same as Fig. 4 in the case of round jets at various azimuthal disturbances: top, $\lambda_\theta/\pi D = 1/3$; middle, $\lambda_\theta/\pi D = 1/4$; bottom, $\lambda_\theta/\pi D = 1/6$. Scalar distributions are on (r, θ) planes.

Fig. 5). However four waves in the inlet disturbance were ultimately suppressed, which is shown in the middle of Fig. 5. Due to this different sensitivity of the roll-up eddies to the azimuthal disturbance, the breakdown of the roll-up eddies in the six-wave case occurs a little closer to the inlet than in the three-wave case. This tendency is more evident in the four-wave case, where a distinct development is not evident and even after the impingement; the flow field is still somehow organized.

In contrast to the round jet, all the plane jet cases tested here show a similar transition independent of the spanwise disturbance. These two figures indicate that, as regards the spanwise or azimuthal instability of a plane or a round impinging jet, the round jet has definite instability modes of $\lambda_\theta/\pi D = 1/6$, while the plane jet show equivalent sensitivity to all modes tested here and the three wavelengths of $\lambda_z/\pi D = 1/3$, 1/4 and 1/6 at the inlet are equally developed.

Another important difference in eddy structures is found in the stagnation region. Fig. 6 indicates the eddy structures of plane and round impinging jets in the stagnation region when the six sinusoidal waves are imposed at the inlet in the spanwise and azimuthal directions respectively. The most notable structures of the plane jet are the elongated twin vortices in a transverse direction (x-direction). This is the famous organized

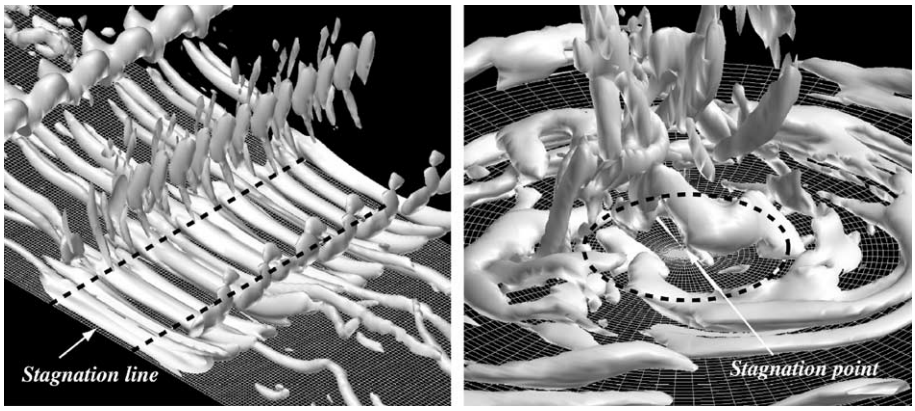

Fig. 6. Instantaneous eddy structures indicated by iso-surfaces of the Laplacian of pressure ($\Delta p' = 4.5$) in the stagnation region of plane (left) and round (right) impinging jets, with six waves imposed at the inlet. A broken line or circle indicates the location of the corresponding nozzle edge at the inlet.

structure observed both experimentally and numerically in the past study (e.g., Yokobori et al., 1983; Sakakibara et al., 1997, 2001, and Tsubokura et al., 1998). This figure also shows that, especially in the case of a plane jet, the structure is not fully developed turbulence but is rather coherent and organized. In contrast to the plane jet, definite organized eddy structures at the stagnation region cannot be identified in the round jet.

The scalar and vorticity, ω_x, distributions on the centre plane ($x/D = 0$) of the plane jets for various spanwise disturbances are shown in Fig. 7. Here it can be seen that the vorticity distributions, given by contour lines, overlap with the mushroom-like scalar distributions, which clearly indicates that substantial amount of scalar is swept away from the near wall region due to these twin vortex pairs. It is also worth noting that the number of mushroom-like scalar distributions and corresponding twin vortex pairings agrees exactly with the spanwise wave number imposed at the inlet.

4.2. Phase-averaged structures

The organized eddy structures arising directly from the inlet temporal disturbance can be easily extracted by using the phase-averaging technique. The phase averaging is taken at $2\pi S_t t = 0 + 2\pi n$, $\pi/2 + 2\pi n$, $\pi + 2\pi n$ and $3\pi/2 + 2\pi n$ in Eq. (6) in which n is a natural number.

Fig. 8 shows phase-averaged vorticity iso-surfaces for streamwise (ω_y), and spanwise (ω_z) or azimuthal (ω_θ) directions (the sample number is about twenty), when six waves in the spanwise or azimuthal directions are imposed at the inlet ($\lambda_z/\pi D = 1/6$). Because the phase-averaged eddy structures of the plane jet are symmetric with respect to the plane, $x/D = 0$, only the positive 'x' region is shown in the figure. In both cases, roll-up eddies caused by the K–H instability are evident and their positions are locked by the phase of the inlet unsteady mode ($2\pi S_t t$). In other words, it can be said that the

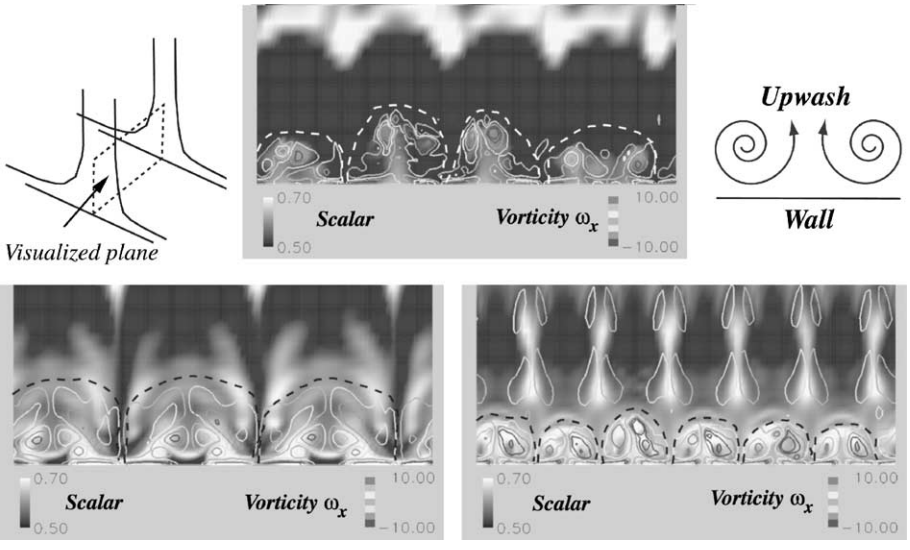

Fig. 7. Instantaneous scalar and vorticity (contour line) distributions of plane jets on the plane $x/D = 0$ at various spanwise disturbances: bottom-left, $\lambda_z/\pi D = 1/3$; top-middle, $\lambda_z/\pi D = 1/4$; bottom-right, $\lambda_z/\pi D = 1/6$. Twin vortices are indicated by a dotted curve.

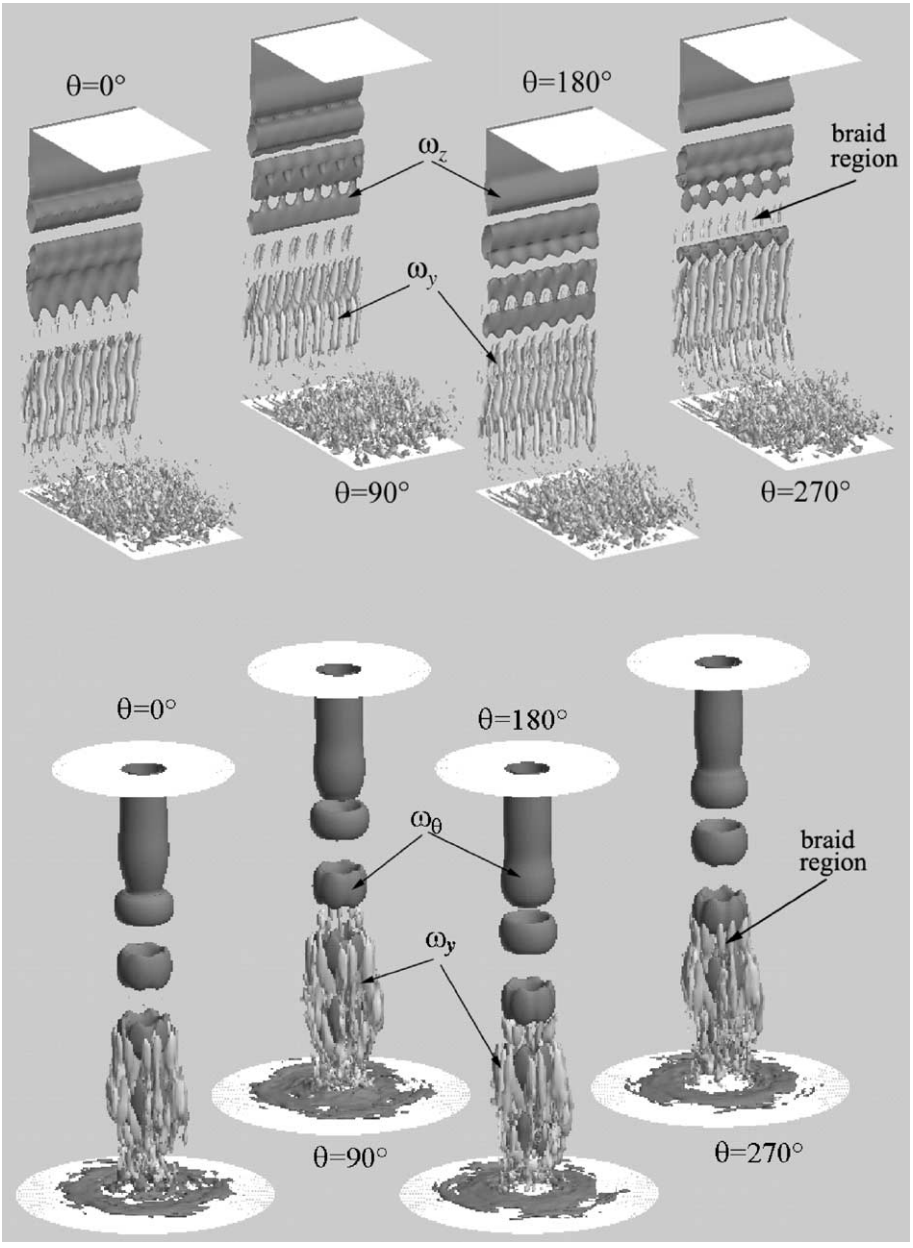

Fig. 8. Iso-surfaces of the phase-averaged vorticity with six waves imposed at the inlet: above two, plane jets, $\omega_z = 1.4$, $\omega_y = \pm 0.5$; below four, round jets, $\omega_\theta = 3$, $\omega_y = \pm 0.5$. The light and dark surfaces indicate positive and negative value respectively.

instability of the free shear layer of both plane and round jets is dominated by the $S_t = 0.4$ imposed at the inlet. The counter-rotating streamwise vortex pairs in the braid region (between the roll-up eddies) are more clearly observed than those shown in the instantaneous images of Figs. 4 and 5. The production of these streamwise vortices in the braid region is known to be caused by the stretching effect (see Fig. 9). That is, the weak streamwise vorticity aligned along the roll-up eddies caused by the instability of shear layer is intensified by the vortex-stretching mechanism between the roll-up eddies rotating in the same direction. In both cases, the number of the pair of the streamwise vortices developed at the braid region is exactly the same as the wave number imposed in the spanwise and azimuthal directions at the inlet (six waves). However it should be noted that, in contrast to the plane jet cases, the round jet shows strong instability at the six-waves. If three or four

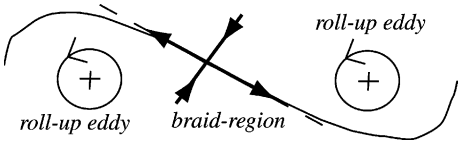

Fig. 9. Schematic images of the stretching at the braid region of a developing jet.

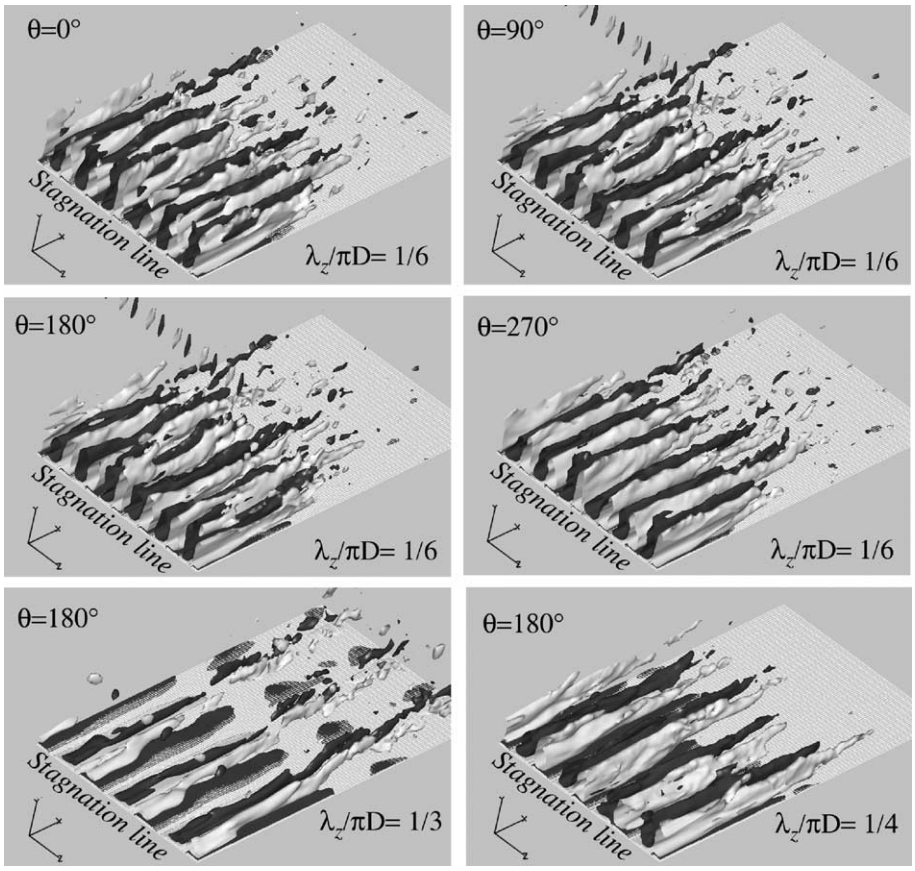

Fig. 10. Iso-surfaces of the phase averaged vorticity at the stagnation region of plane jets ($\omega_x = \pm 1.0$): above four, $\lambda_z/\pi D = 1/6$ at four different phases; below-left, $\lambda_z/\pi D = 1/3$ at $\theta = 180°$; below-right, $\lambda_z/\pi D = 1/4$ at $\theta = 180°$. The light and dark surfaces indicate positive and negative value respectively.

waves are imposed at the inlet, then the three waves are developed to six and the four waves do not develop at all, as has already been shown in Fig. 5.

In the previous section, we have observed the twin vortices in the stagnation region of the plane jet in Figs. 6 and 7. To investigate these characteristic eddies more intensively, the phase-averaged vorticity, ω_x, in the stagnation region of the plane jet is displayed in Fig. 10. A strong counter-rotating elongated vortex pair can be seen in the vicinity of the impingement on the wall. It seems that the twin vortices exist not intermittently but rather continuously in the stagnation region. From Figs. 9 and 10 it is clear that the twin vortices in the stagnation region are strongly related to the counter-rotating streamwise vortices observed in the braid region of the plane jet and the number of pairs of these vortices is exactly the same as the wave number of the spanwise disturbance imposed at the inlet.

5. Dependence on Reynolds number

The dependence of the eddy structures on the Reynolds number of the plane impinging jet is investigated here with the characteristic twin vortices in the stagnation region of plane jets being of main concern. Accordingly the higher Reynolds number case of 6000 is studied using LES in this section. The accuracy of LES in the plane jet is demonstrated by comparisons with experimental data in Tsubokura et al. (1997).

Fig. 11 shows comparisons of phase-averaged vorticity for spanwise (ω_z) and streamwise directions (ω_y) at Reynolds numbers of 2000 and 6000, for two spanwise disturbances of $\lambda_z/\pi D = 1/3$ and 1/4 at the inlet. Compared with the low Reynolds number case, the high Reynolds number case shows rather faster transition to turbulence and the development of the streamwise counter-rotating vortices at the braid is found to be enhanced. However this earlier stage of transition also seems to be dominated by the spanwise disturbance and the number of counter-rotating vortex pairs is the same as the inlet wave number, though the streamwise vortex pair in the higher Reynolds number case is rather indistinct perhaps due to the distortion of the surrounding turbulence. The flow-fields in the stagnation region at higher Reynolds numbers also show less organized and coherent structures than the ones at the lower Reynolds number.

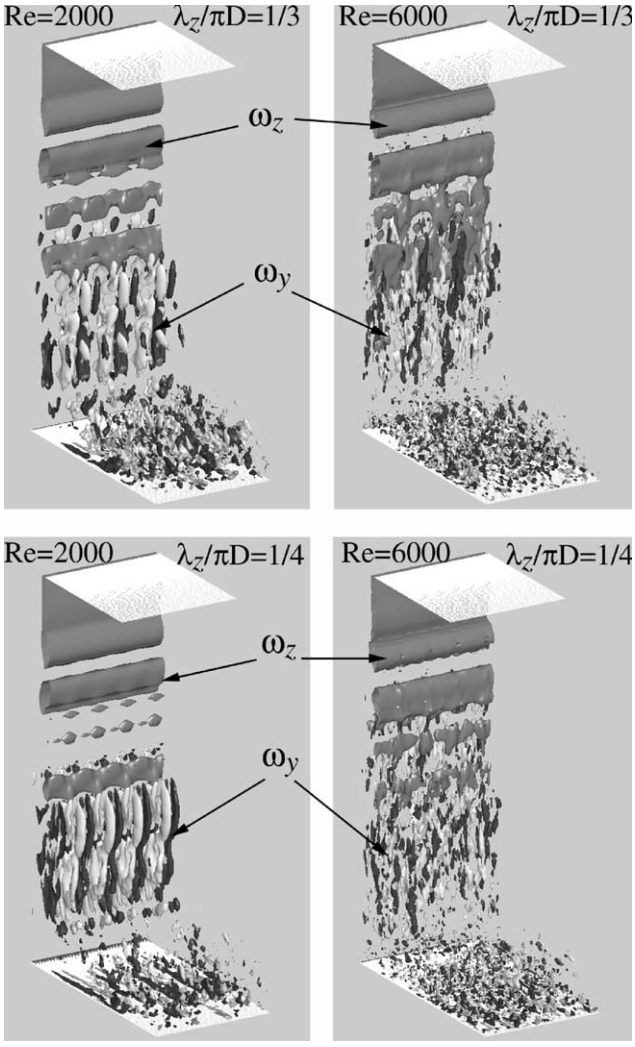

Fig. 11. Iso-surfaces of the phase-averaged vorticity of plane jets at $\theta = 180°$ at different Reynolds numbers ($\omega_z = 1.45$; $\omega_y = \pm 0.4$): two on the top, $\lambda_z/\pi D = 1/3$; two on the bottom, $\lambda_z/\pi D = 1/4$. The light and dark surfaces indicate positive and negative value respectively.

As regards the number of twin vortices in the stagnation in this rather highly turbulent state, Figs. 12 and 13 show phase-averaged vorticity for the x-direction and its instantaneous distributions at higher Reynolds number case respectively. Compared with the lower Reynolds number cases, phase-averaged twin vortices at the stagnation region are rather indistinct and their positions are seemingly not well fixed along the spanwise direction, as is shown in Fig. 12. However this does not necessarily imply that the twin vortices are weaker at the higher Reynolds number. In fact we can observe definite twin vortices in the snapshot of Fig. 13 at the higher Reynolds number (indicated by the dotted curve), which is rather distorted due to the surrounding turbulence compared with the ones shown in Fig. 7. It is worth noting that the top of Fig. 13 indicates the four pair of the twin vortices, even though three waves are imposed at the inlet ($\lambda_z/\pi D = 1/3$), while rather intensive four pairs of twin vortices are observed on the bottom of Fig. 13 when four waves are imposed ($\lambda_z/\pi D = 1/4$). It should be noted that the spanwise perturbation at the inlet is only 0.5% of the inlet velocity V_0. Considering this fact, it can be concluded that the effect of producing the same number of twin vortices in the stagnation region as the spanwise wave number imposed at the inlet seems to be suppressed by the spanwise natural instability at the higher Reynolds number.

6. Concluding remarks and discussion

The findings of the present study can be summarized as follows:

(1) The development or transition of both plane and round jets is similar in the sense that roll-up eddies appearing near the nozzle show spanwise or azimuthal instability as the flow develops downstream and a streamwise counter rotating vortex pair grows in the braid region. The round jet shows definite instability modes for the azimuthal direction ($\lambda_\theta/\pi D = 1/6$), while the plane jet shows equivalent sensitivity to all modes and the three wavelengths of $\lambda_z/\pi D = 1/3$, 1/4 and 1/6 imposed at the inlet in the spanwise direction are equally developed.
(2) Eddy structures near the stagnation point are different for plane and round jets. The plane jet shows organized structures such as twin vortices counter-rotating in the transverse direction of the jet. The number of the twin vortices agrees well with the wave number imposed at the inlet. In contrast, no definite organized structures in the stagnation region are evident for the round jet.
(3) In the plane jet case, the development of the jet is enhanced for the higher Reynolds number case. Due to this earlier transition, the twin vortices in the stagnation region are rather distorted and perturbed by the surrounding turbulence.

The difference in the eddy structures at the stagnation region can be explained by the difference in the stretching directions between plane and round jets on a wall. In the case of the plane jet, strong stretching is caused in the transverse direction (x-direction) by the acceleration of the flow after impingement due to the high pressure in the stagnation region, as well as by the counter-rotating roll-up eddies moving apart across the stagnation line after impingement, while little stretching or shrinking occurs in the spanwise direction. Therefore a small transverse perturbation imposed upstream of the jet is strongly intensified in the stagnation region and twin vortices are produced. In the case of the round jet, the flow does not accelerate much in the r-direction because of the expansion of the flow field after

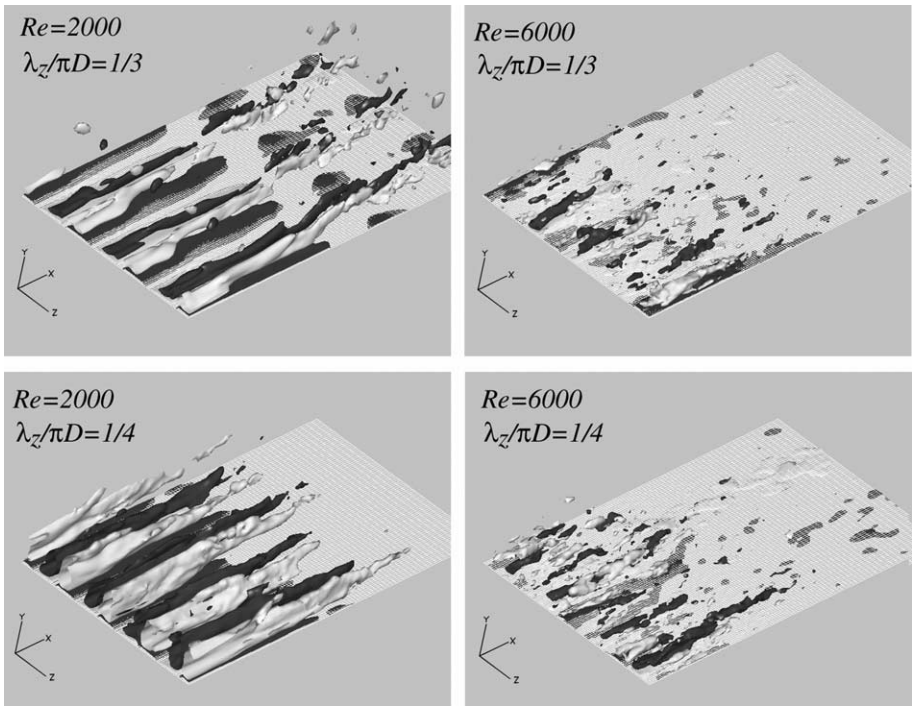

Fig. 12. Iso-surfaces of the phase-averaged vorticity near the impinging wall at $\theta = 180°$ at different Reynolds numbers ($\omega_x = \pm 1.2$): two on the top, $\lambda_z/\pi D = 1/3$; two on the bottom, $\lambda_z/\pi D = 1/4$. The light and dark surfaces indicate positive and negative value respectively.

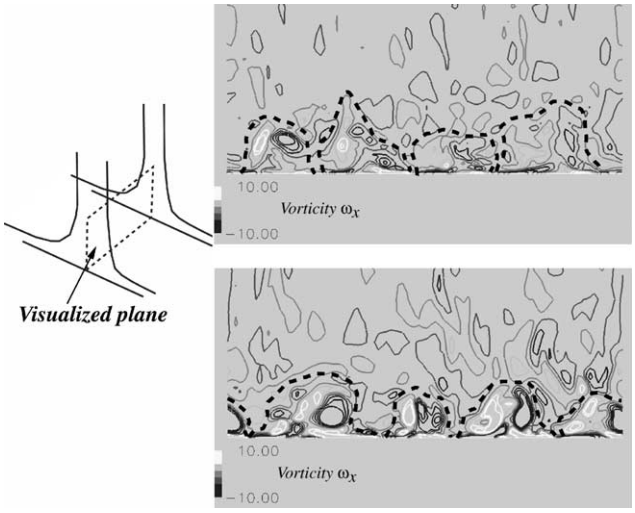

Fig. 13. Instantaneous vorticity distribution in the transverse direction (ω_x) of plane jets on the plane $x/D = 0$ at the Reynolds number of 6000: top, $\lambda_z/\pi D = 1/3$; bottom, $\lambda_z/\pi D = 1/4$. Twin vortices are indicated by a dotted curve.

the impingement and azimuthal stretching dominates the flow field. Therefore only the roll-up eddies with the rotating axis in the θ-direction are enhanced.

As regards the instability of plane and round impinging jets for spanwise and azimuthal disturbances respectively, previous works on vortex rings in mixing layers and round jets may help. According to the experimental study of a plane free shear layer conducted by Lasheras and Choi (1988), it was found that many spanwise wavelengths are equivalently excited. The results obtained here also support this conclusion, even though it has been found that a plane impinging jet without any inlet spanwise disturbance has a natural unstable mode of $\lambda_z/\pi D = 1/4$ for the spanwise direction in the case of $S_t = 0.4$. It seems that in a plane jet, the most unstable mode is determined by the streamwise forcing frequency, but it is not so dominant as to suppress the other spanwise modes and many disturbances are equivalently developed.

In addition to the streamwise forcing frequency, the ratio of the radius and the shear-layer thickness (R/θ) or the core of the vortex ring (R/δ) becomes an important factor in determining the instability mode for the azimuthal direction of the round jet. In addition to the helical mode at the far downstream of an axisymmetric jet found by Batchelor and Gill (1962) from the linear stability theory, a large number of azimuthal modes are unstable in the thin axisymmetric shear layer (Cohen and Wygnanski, 1987). The vortex ring simulation using a 3D vortex element method conducted by Ghoniem and Knio (1987) showed that vortex rings become unstable to a particular azimuthal perturbation that depends on a core to radius ratio of the vortex ring. They found that a wavenumber of six for the azimuthal direction became unstable for a core to radius ratio of 0.35, while decreasing the ratio increases the unstable wave number. Considering these previous works, the

definite instability observed in our round impinging jet seems to be reasonable.

Many researchers have pointed out that the twin vortices observed in the stagnation region of plane jets play an important role in establishing the high heat and mass transfer rates near the wall impingement point (Yokobori et al., 1983; Sakakibara et al., 1997, 2001). The knowledge obtained in this study definitely indicates the possibility of controlling heat and mass transfer rates near the stagnation region of the plane jet by regulating the inlet forcing conditions.

References

Batchelor, G.K., Gill, A.E., 1962. Analysis of the stability of axisymmetric jets. J. Fluid Mech. 14, 529–551.

Cohen, J., Wygnanski, I., 1987. The evolution of instabilities in the axisymmetric jet. Part I. The linear growth of disturbances near the nozzle. J. Fluid Mech. 176, 191–219.

Germano, M., Piomelli, U., Moin, P., Cabot, W.H., 1991. A dynamic subgrid-scale eddy viscosity model. Phys. Fluids A 3, 1760–1765.

Ghoniem, A.F., Knio, O.M., 1987. Three dimensional vortex simulation with application to axisymmetric shear layers, AIAA paper 87-0379.

Lasheras, J.C., Choi, H., 1988. Three-dimensional instability of a plane free shear layer: an experimental study of the formation and evolution of streamwise vortices. J. Fluid Mech. 189, 53–86.

Lilly, D.K., 1992. A proposed modification of the Germano subgrid-scale closure method. Phys. Fluids A 4, 633–635.

Martin, H., 1977. Heat and mass transfer between impinging gas jets and solid surface. Adv. Heat Transfer 13, 1–60.

Meneveau, C., Lund, T.S., Cabot, W.C., 1996. A Lagrangian dynamic subgrid-scale model of turbulence. J. Fluid Mech. 319, 353–385.

Pierrehumbert, R.T., Widnall, S.E., 1982. The two- and three-dimensional instabilities of a spatially periodic shear layer. J. Fluid Mech. 114, 59–82.

Sakakibara, J., Hishida, K., Maeda, M., 1997. Vortex structure and heat transfer in the stagnation region of an impinging plane jet. Int. J. Heat Mass Transfer 40 (13), 3163–3176.

Sakakibara, J., Hishida, K., Phillips, R.C., 2001. On the vortical structure in a plane impinging jet. J. Fluid Mech. 434, 273–300.

Satake, S., Kunugi, T., 1998. Direct numerical simulation of an impinging jet into parallel disks. Int. J. Numer. Meth. Heat Fluid Flow 8 (8), 768–780.

Sutera, S.P., Maeder, P.F., Kestin, J., 1963. On the sensitivity of heat transfer in the stagnation-point boundary layer to free-stream vorticity. J. Fluid Mech. 16, 497–520.

Sutera, S.P., 1965. Vorticity amplification in stagnation-point flow and its effect on heat transfer. J. Fluid Mech. 21 (3), 513–534.

Tsubokura, M., Kobayashi, T., Taniguchi, N., 1996. An investigation of the localized dynamic mixed SGS model and its application to turbulent channel flow. Trans. JSME ser. B 62 (601), 3292–3299 (in Japanese).

Tsubokura, M., Kobayashi, T., Taniguchi, N., 1997. Large eddy simulation of plane impinging jets. Proc. 11th Symp. on Turbulent Shear Flow. Grenoble, pp. 2224–2229.

Tsubokura, M., Kobayashi, T., Taniguchi, N., 1998. Visualization of 3-D structures at a stagnation region of a plane impinging jet using large eddy simulation. Proc. 8th Int. Symp. on Flow Visualization, Sorrent, no. 291, in CD-ROM.

Tsubokura, M., 2001. Proper representation of the subgrid-scale eddy viscosity for the dynamic procedure in large eddy simulation using finite difference method. Phys. Fluids 13 (2), 500–504.

Yokobori, S., Kasagi, N., Hirata, M., 1983. Transport phenomena at the stagnation region of a two-dimensional impinging jet. Trans. JSME ser. B 49 (441), 1029–1039.

Yoshizawa, A., Tsubokura, M., Kobayashi, T., Taniguchi, N., 1996. Modeling of the dynamic subgrid-scale viscosity in large eddy simulation. Phys. Fluids 8 (8), 2254–2256.